Journal of Solid State Electrochemistry (2019) 23:837–846
https://doi.org/10.1007/s10008-018-04187-0

ORIGINAL PAPER

Beneficial effect of phase transition on kinetics of deintercalation/intercalation process in lithium–manganese spinel

Łukasz Kondracki [1,2] · Janina Molenda [1,2]

Received: 7 June 2018 / Revised: 14 November 2018 / Accepted: 25 December 2018 / Published online: 6 January 2019

Abstract

In this work, a detailed characterization of $Li_xMn_2O_4$ spinel oxides is shown to demonstrate the correlation between the anomalous thermoelectric properties of this cathode material and its crystal and electronic structure. The analysis of structural and transport in $Li_xMn_2O_4$ cathode materials obtained by solid-state reaction and sol–gel method allows formulating a conclusion that the performance of manganese spinel-based cathode depends on the occurrence of anomalous electron effects. The recorded maxima in absolute values of thermoelectric power correspond to high diffusivity of electrons at the Fermi level. A correlation between the occurrence of thermoelectric peaks and effectiveness of deintercalation/intercalation of lithium has been shown. The obtained results indicate a beneficial effect of phase transition on electrochemical properties of lithium–manganese spinel cathode material.

Keywords Electrochemical deintercalation · Manganese spinel · Electrical properties

Introduction

Manganese spinel, less expensive and environmentally friendlier than presently used in Li-ion batteries technology $LiCoO_2$ oxide, seems to be an alternative cathode material. The $Li_xMn_2O_4$ manganese spinel owes its properties to a wide lithium content range that can be changed between 0 and 1 without crucial changes in the spinel structure of this oxide [1–3]. Diffusional lithium deintercalation/intercalation mechanism is the basis for its application as an electrode in a rechargeable battery.

At around 290 K, manganese spinel undergoes a phase transition from cubic to orthorhombic phase [4, 5] resulting in the ordering of manganese in the *3d* metal sublattice. Many authors believe that this Jahn-Teller driven structural distortion is the reason for the insufficient cyclability of the manganese spinel-based batteries [6, 7]. In spite of a large number of works dealing mostly with electrochemical characteristics of lithium cells with $LiMn_2O_4$-based cathode materials [8–17], only few focuses on anomalous electronic effects near the temperature of the phase transition [18–22].

DFT calculations of both spinel phases by Grechnev et al. [23, 24] reveal a significant difference in the density of states near Fermi level between cubic and orthorhombic phase.

The purpose of this work is an attempt to relate the anomalous effects in thermoelectric power with the structural transition and electrochemical performance of spinel-based cathode materials. In order to accomplish this, detailed structural studies as a function of temperature for lithium–manganese spinels $Li_xMn_2O_4$ were carried out for a different lithium content.

Experimental

Lithium–manganese spinel oxides were synthesized using both solid-state reaction (*SSR*) [25] as well as sol–gel method (*SG*) described in details in [26]. The materials were then annealed in air at 800 °C for 24 h (solid-state reaction) and

Electronic supplementary material The online version of this article (https://doi.org/10.1007/s10008-018-04187-0) contains supplementary material, which is available to authorized users.

✉ Janina Molenda
molenda@agh.edu.pl

[1] AGH University of Science and Technology, Faculty of Energy and Fuels, Department of Hydrogen Energy, al. A. Mickiewicza 30, 30-059 Krakow, Poland

[2] AGH University of Science and Technology, AGH Centre of Energy, ul. Czarnowiejska, 36, 30-054 Krakow, Poland

6 h (sol–gel method) followed by quenching to room temperature. The obtained powders were pressed into pellets which served as cathodes in $Li|Li^+|Li_xMn_2O_4$ cells. In the characteristic point on the charge curve, the loading process was stopped to obtain materials with a different degree of lithium content.

X-ray diffraction measurements (XRD) were performed in 2θ range of 10–110° with CuK_α radiation using the PANalytical Empyrean diffractometer. For structural characterization of the materials as a function of temperature, Oxford Cryostat and Anton Paar furnace setups were used. The XRD data were refined using the Rietveld method, with GSAS/EXPGUI set of software [27].

For the measurements of electrical conductivity (σ) of the samples, a four-probe AC method was utilized in the range of 218 to 328 K. Measurements of thermoelectric power (α) were performed in the same temperature range using a dynamic method with variable temperature gradient.

Charge–discharge test as well as the determination of chemical lithium diffusion coefficients was carried out in CR-2032 $Li|Li^+|Li_xMn_2O_4$ cells, with composite cathodes consisting of active material, carbon black, and PVDF (with a weight ratio of 8:1:1 respectively). $LiPF_6$ salt in EC/DEC was used as an electrolyte. The cells were cycled with a current regime in the range of C/10 to 10 C with voltage cutoffs set as 3.5 and 4.3 V. The measurements of chemical diffusion

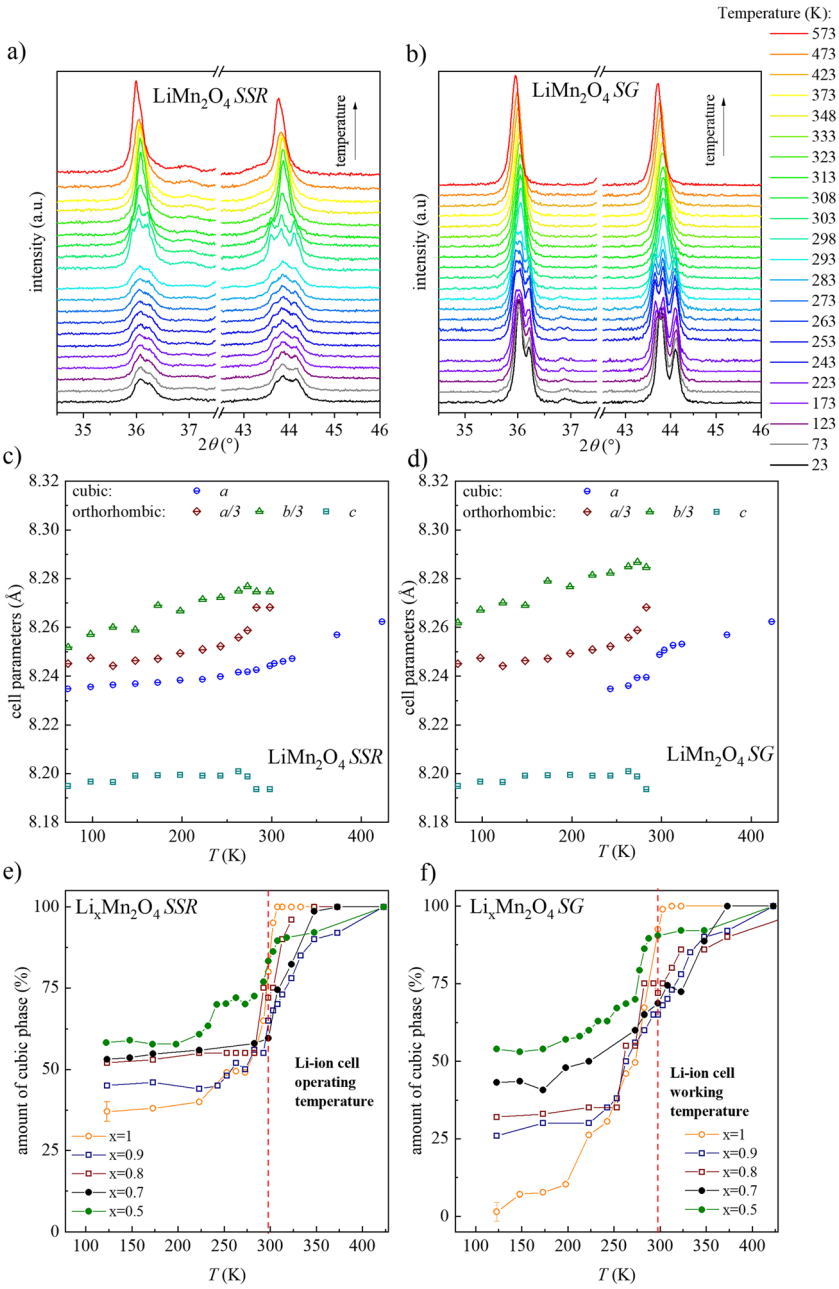

Fig. 1 Enlargement of XRD patterns of $LiMn_2O_4$ obtained by the following: **a** solid-state reaction (*SSR*), **b** sol–gel method (*SG*). Evolution of lattice cell parameters of $LiMn_2O_4$ **c** *SSR* and **d** *SG*. Phase transition: cubic → orthorhombic in electrochemically deintercalated $Li_xMn_2O_4$ **e** *SSR*, **f** *SG*. For increasing the clarity of the graph, a mean error value was marked for one point. The red line indicates Li-ion cell working temperature

coefficients of lithium were carried out using galvanostatic intermittent titration technique [28] at room temperature.

Results and discussion

Structural studies of $Li_xMn_2O_4$

The pristine materials obtained from both synthesis routes (solid-state reaction and sol–gel), as well as the materials with a different lithium contend obtained via electrochemical deintercalation were structurally examined in 23–573-K temperature range in order to monitor the phase transition. With the use of Rietveld refinement method, lattice cell parameters, as well as phase composition of the materials, was determined. In Fig. 1a, detailed results of structural studies of $LiMn_2O_4$ obtained by a solid-state reaction are shown along with results of Rietveld refinement (Fig. 1c and e).

A spinel cubic phase with the $Fd\bar{3}m$ space group is shown to exhibit single, sharp diffraction peaks for the temperature above 313 K. Below this temperature, the peak splits into three, what indicates an appearance of the second phase, indexed with *Fddd* space group. The cubic/orthorhombic ratio drops rapidly, reaching the value of 1:1 around room temperature (Fig. 1e, orange points). The phase transition, however, does not undergo completely, below 250 K the phase ratio is constant, with 30% of cubic phase. A linear change of cubic phase cell parameters was observed in the whole examined range.

Detailed structural studies of $LiMn_2O_4$ *SG* together with results of Rietveld analysis are given in Fig. 1b. For this pristine material, phase transition is complete and occurs in 10 degrees lower temperature than for material from solid-state reaction. Below 123 K, only the orthorhombic *Fddd* phase is present (Fig. 1f).

The same examining procedure was carried out for electrochemically deintercalated manganese spinel materials both from solid-state reaction and from sol–gel method. Figure 1e illustrates the phase transition in the material from solid-state reaction as a function of temperature and lithium content. The temperature of the phase transition increases with the decrease of lithium content, the transition is also smoother, what results in higher amount of cubic phase in a lower temperature for materials with lower lithium concentration. For the materials obtained by partial lithium deintercalation from $LiMn_2O_4$ *SG*, the phase transition is

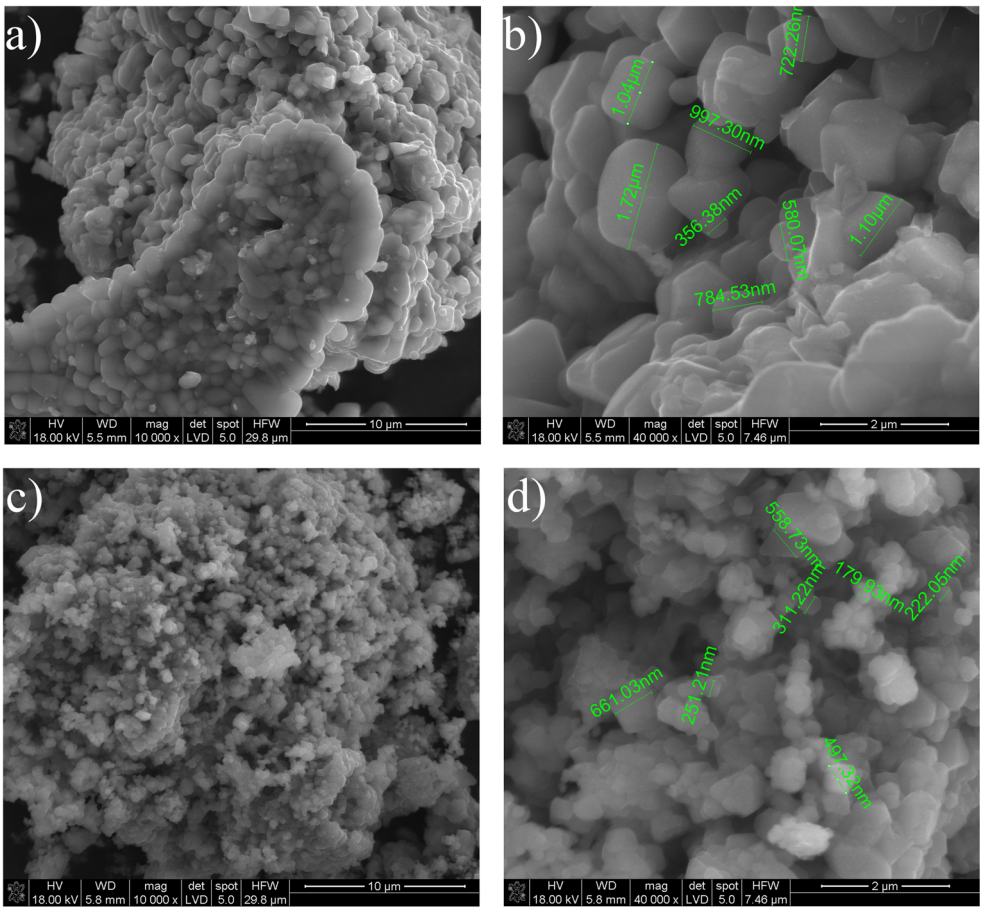

Fig. 2 SEM images of the $LiMn_2O_4$ powder microstructure obtained by solid-state reaction, (*SSR*) with a magnification of **a** × 10,000, **b** × 40,000. SEM images of the $LiMn_2O_4$ powder microstructure obtained by sol–gel (*SG*) method, with a magnification of **c** × 10,000, **d** × 40,000

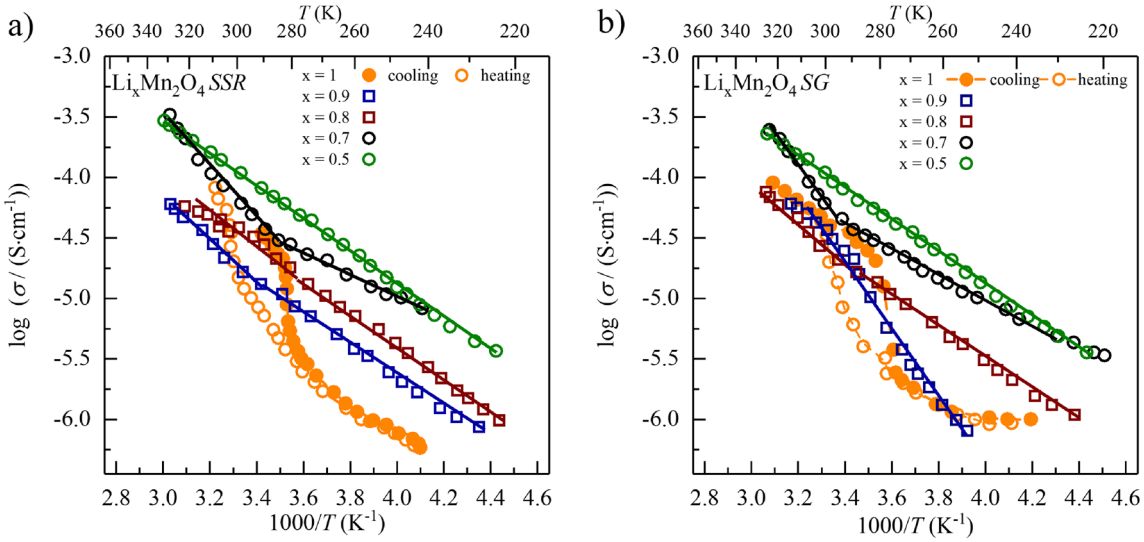

Fig. 3 Temperature dependence of electrical conductivity of the following: **a** pristine $LiMn_2O_4$ *SSR* and after partial lithium deintercalation, **b** pristine $LiMn_2O_4$ *SG* and after partial lithium deintercalation

smoother than in materials derived from $LiMn_2O_4$ *SSR* and is shifted towards lower temperature (Fig. 1f).

The obtained results indicate that the applied synthesis route (*SSR* or *SG*) affects the temperature of the phase transition and the composition of the phases of manganese spinel-based cathode material. Distinct from the solid-state reaction approach, the mixing of substrates in sol–gel method is performed at an atomic level, in our case at room temperature, what allows to shorten the time of the annealing process necessary to obtain a lithium–manganese oxide with a desired spinel phase. The differences of annealing times affect the small amounts of lithium that evaporate during the synthesis, what can slightly affect the stoichiometry of obtained materials, resulting in a shift of the temperature the of phase transition.

Table 1 Activation energy values of conductivity of $Li_xMn_2O_4$ obtained by electrochemical deintercalation of lithium from materials from solid-state reaction and sol–gel method

Composition	Solid-state reaction		Sol–gel method	
	Temperature range (K)	E_a (eV)	Temperature range (K)	E_a (eV)
$LiMn_2O_4$	283–293	0.34	283–323	0.30
	243–273	0.32	253–273	0.29
$Li_{0.9}Mn_2O_4$	228–318	0.32	253–298	0.34
$Li_{0.8}Mn_2O_4$	273–313	0.29	223–328	0.28
	228–273	0.28		
$Li_{0.7}Mn_2O_4$	293–328	0.28	223–283	0.28
	228–293	0.27	283–323	0.30
$Li_{0.5}Mn_2O_4$	223–328	0.27	223–328	0.26

Microstructure

Figure 2 a and b show the morphology of the $LiMn_2O_4$ powder synthesized using the high-temperature method. A polycrystalline material with diverse microstructure was obtained. Agglomerates with diameters above 10 μm have been observed (Fig. 2a), while grain sizes are 0.5–2 μm. Inter-grain boundaries are clearly visible.

Figure 2 c and d show the morphology of the $LiMn_2O_4$ powder synthesized using the sol–gel method. A polycrystalline material with diverse microstructure was obtained. In the case of this material, also larger agglomerates with diameters above 10 μm have been observed (Fig. 2c), grain sizes are noticeably smaller, amounting to 0.2–0.7 μm. It is believed that this phenomenon is due to the fact that the annealing process was much shorter in case of the sol–gel synthesis route. This *(SG)* material was annealed in 800 °C for 6 h, what resulted in obtaining of much smaller grains than in the case of material from solid-state reaction *(SSR)*, where the annealing process lasted 24 h.

Transport properties

Conductivity

The results of conductivity measurements of pristine $LiMn_2O_4$ *SSR* and the materials obtained after its electrochemical deintercalation are shown in Fig. 3a. The observed conductivity vs. temperature dependence in the Arrhenius plot exhibits an activated character, what allowed to calculate activation energy.

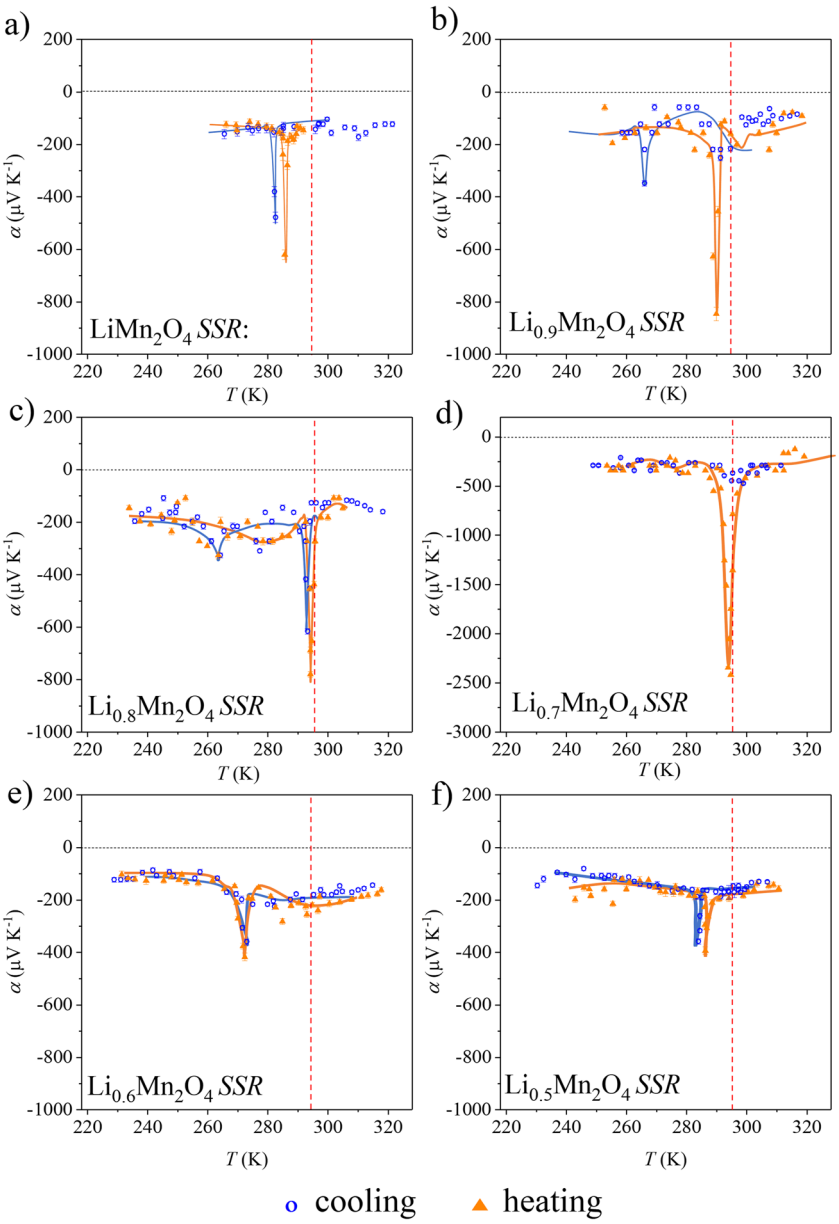

Fig. 4 Temperature dependence of thermoelectric power of $Li_xMn_2O_4$ obtained by electrochemical deintercalation of $LiMn_2O_4$ from solid-state reaction: **a** pristine material, **b** $x = 0.9$, **c** $x = 0.8$, **d** $x = 0.7$, **e** $x = 0.6$, **f** $x = 0.5$. The red vertical line indicates Li-ion cell working temperature

Pristine material exhibits a specific hysteresis in the temperature characteristic of conductivity, connected with cubic → orthorhombic phase transition. The latter exhibits lower conductivity. For the deintercalated materials, identical results were obtained during cooling and heating cycle (Fig. S1 in supplementary material), the hysteresis disappeared; however, changes in the activation energy were visible. With the decrease of lithium content, an increase in conductivity was observed in the whole examined temperature range, what can be ascribed to a higher content of better conducting cubic phase (Fig. 1e). Analogous measurements were carried out for pristine $LiMn_2O_4$ *SG* and the materials obtained after its electrochemical deintercalation are shown in Fig. 3b.

Similar to the material from solid-state reaction, the one from sol–gel method exhibits a distinctive hysteresis in the temperature characteristic of conductivity, connected with phase transition, however, shifted towards lower temperature, what is consistent with structural studies (lower temperature of phase transition for $LiMn_2O_4$ *SG*). The conductivity increases with the lithium deintercalation degree; calculated activation energies of electrical conductivity are presented in Table 1.

In case of all the measured samples, very high values of linear correlation were obtained, and the error of E_a does not exceed 0.01 eV. The phase transition affects also the conductivity of the sample; hence, depending on the phase ratio, one sample can have more than one activation energies in the measured temperature range, so there is no general linear dependency of chemical composition and activation energy; however, it can be observed that with the increase of lithium deintercalation degree, a decrease in activation energy and a decrease of lattice cell

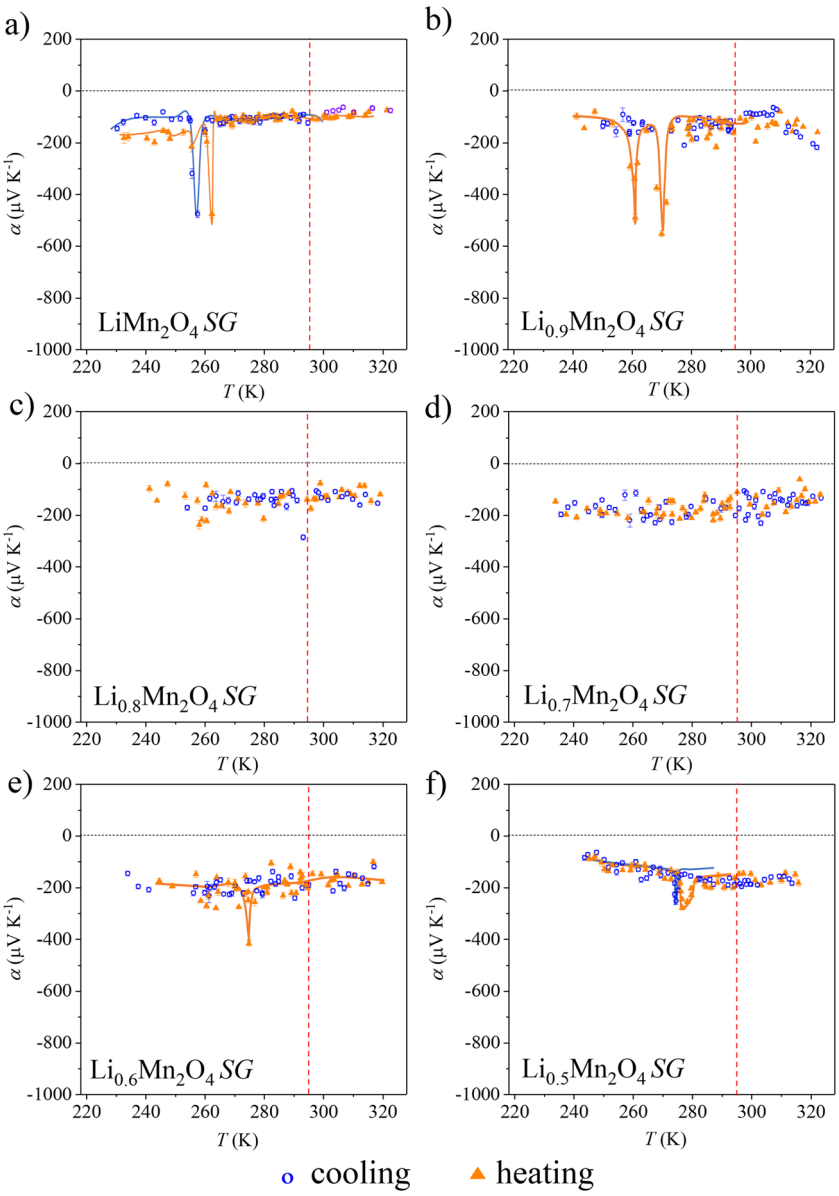

Fig. 5 Temperature dependence of thermoelectric power of $Li_xMn_2O_4$ obtained by electrochemical deintercalation of $LiMn_2O_4$ from sol–gel method: **a** pristine material, **b** $x = 0.9$, **c** $x = 0.8$, **d** $x = 0.7$, **e** $x = 0.6$, **f** $x = 0.5$. Red vertical line indicates Li-ion cell working temperature

parameters were observed. Together with results of thermoelectric power, it indicates on polaron as the mechanism of charge transport, regardless of synthesis method.

Thermoelectric power

In Fig. 4, results of thermoelectric power measurements of $Li_xMn_2O_4$ *SSR* are shown as a function of temperature and lithium content.

For the pristine $LiMn_2O_4$ material, a sharp -600 μV K^{-1} peak in the thermoelectric power was obtained (Fig. 4a) around 283 K, both during cooling and heating of the sample. This behavior (thermoelectric peak) does not find a theoretical explanation and can be attributed to the phase transition. Negative values of the thermoelectric power in the whole examined temperature range indicate that electrons are the predominant charge carriers. For $Li_{0.9}Mn_2O_4$ *SSR*, a sharp -900 μV K^{-1} peak during heating was observed (Fig. 4b) around room temperature. The highest absolute value of the peak was observed for $x = 0.7$ (-2500 μV K^{-1}). For higher degrees of deintercalation $x \leq 0.6$, the effects are not as visible, and shifted towards lower temperatures.

The same measurement procedure was carried out for electrochemically deintercalated materials obtained from the spinel from sol–gel method ($LiMn_2O_4$ *SG*). The results are shown in Fig. 5.

Similarly to the pristine material from solid-state reaction, in the one from sol–gel method, the anomalous effects (peaks of value -500 μV K^{-1}) in thermoelectric power were observed; however, they were shifted towards lower temperature 260 K. These results are in a good agreement with structural and conductivity studies. Electrochemically deintercalated

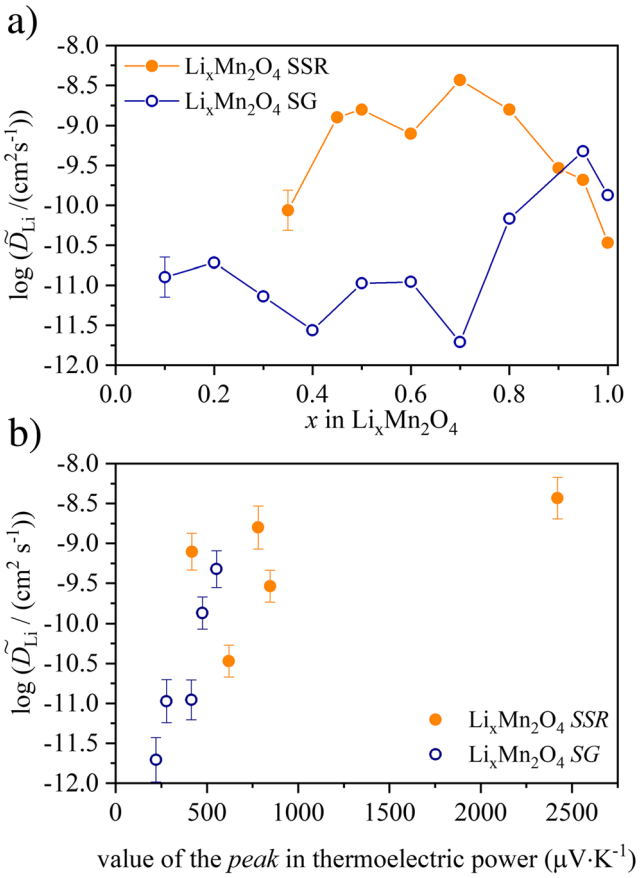

Fig. 6 **a** Lithium chemical diffusion coefficient as a function of lithium content x in $Li_xMn_2O_4$ cathode materials obtained by solid-state reaction and sol–gel method. To increase the clarity of the plot, the mean error was marked for one point. **b** Correlation between chemical diffusion coefficient of lithium and values of thermoelectric peak for $Li_xMn_2O_4$

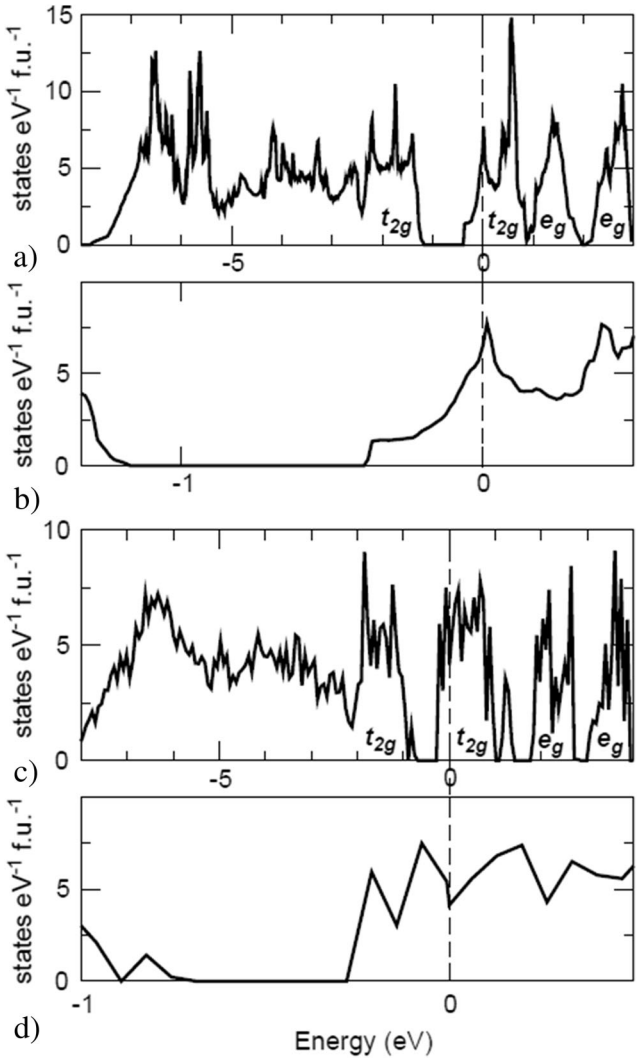

Fig. 7 Densities of states for the AFM $LiMn_2O_4$ in the spinel (**a** total DOS; **b** finer structure of DOS at E_F) and the orthorhombic structure (**c** total DOS; **d** finer structure of DOS at E_F) [24]. Reprinted from Journal of Magnetism and Magnetic Materials, 258, G.E. Grechnev, R. Ahuja, B. Johansson, O. Eriksson, *Electronic structure and magnetic properties of lithium manganese spinels*, 287–289, Copyright (2018), with permission from Elsevier

$Li_{0.9}Mn_2O_4$ exhibited two sharp peaks in the characteristic (Fig. 5b), again shifted towards lower temperatures. Materials with lower lithium content (Fig. 5c–f) did not exhibit such significant peaks.

These distinctive peaks in thermoelectric power appear in the temperature of phase transition, where cubic to orthorhombic phase ratio is 1:1.

Lithium diffusion coefficient

The results of lithium diffusion coefficients for both spinel materials obtained by GITT method are shown in Fig. 6. The obtained results of lithium diffusion coefficient D are consistent with data found in literature derived from different techniques: GITT [29, 30], PITT [31, 32], and EIS [33] (see Tab. S1. in Supplement) with a characteristic minimum around $x = 0.7$ for $LiMn_2O_4$ obtained from sol–gel method from this work.

In the examined range of lithium content, $Li_xMn_2O_4$ obtained by a solid-state reaction exhibits higher diffusion coefficient than the material from sol–gel method. It would seem that taking into consideration the size of the grains in both materials, one could expect a different result (shortening the lithium diffusion path for smaller grains from sol–gel method). It is probable that much better kinetics of the process of lithium deintercalation/intercalation can be connected with the occurrence of phase transition. The material obtained in sol–gel method undergoes the phase transition in temperatures 10–20 degrees lower than room temperature; it also exhibits much lower absolute values of anomalous thermoelectric effects. It is believed that the differences in the lithium diffusion coefficient at different lithium content can be attributed to the differences in the anomalous thermoelectric power characteristics at around room temperature introduced by the phase transition and phase ratio Fddd: $Fd\bar{3}m$ 1:1. The most significant difference in the lithium diffusion

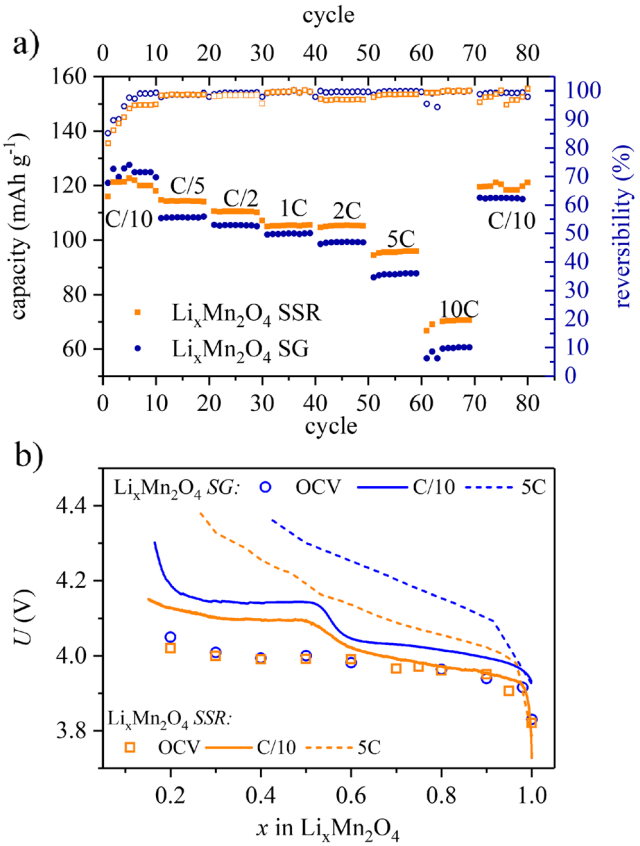

Fig. 8 **a** Discharge capacity of Li|Li$^+$|Li$_x$Mn$_2$O$_4$ with reversibility of charge/discharge processes as a function of cycle numbers for various current loads. Hollow points correspond to reversibility (right axis), filled to capacity (left). **b** Charge curves of Li|Li$^+$|Li$_x$Mn$_2$O$_4$ (OCV and under load) with cathode materials from solid-state reaction and sol–gel method

coefficient in both materials is observed for the composition $x = 0.7$, for which the highest value of peak in thermoelectric power was recorded (-2500 μV K^{-1}). The observed maxima in absolute values of Seebeck coefficient denote high electron diffusivity at the Fermi level—where charge transfer occurs during electrode process. It has been demonstrated that the material from solid-state reaction exhibits anomalous thermoelectric effects closer to the Li-ion cell working temperature than in the case of material from sol–gel method, what most probably is the reason for better kinetics of lithium deintercalation/intercalation.

To explain these phenomena, calculations of electronic structure done by Grechnev et al. [23, 24] turned out to be of great help. The Fermi level of cubic phase of LiMn$_2$O$_4$ is located in a local maximum of density of states (DOS), while for the orthorhombic phase, it is located in local minimum of DOS (Fig. 7). This severe difference in density of states in both coexisting phases is the reason behind the anomalous thermoelectric effects and high diffusivity of electrons affecting lithium deintercalation/intercalation process.

Precise crystal structure studies revealed that the temperature in which significant thermoelectric peaks appear corresponds to the temperature in which ratio of coexisting phases is 1:1. Figure 6b illustrates a correlation between lithium chemical diffusion coefficient and values of thermoelectric peaks. It can be seen that the increase in value of the peak leads to higher values of lithium chemical diffusion coefficient.

Electrochemical properties

Figure 8a presents discharge capacities of Li|Li$^+$|Li$_x$Mn$_2$O$_4$ cells with cathode materials from both compared method of synthesis. The cells were charged and discharged with a current of C/10, C/5, C/2, 1 C, 2 C, 5 C, and 10 C. For each current value, first 10 cycles were recorded.

The electrochemical tests revealed a similar discharge capacity around 120 mAh g^{-1} for both materials with C/10 current. However, the material from solid-state reaction exhibits higher capacities while discharged with higher currents (C/5–10 C). In Fig. 8b, a comparison of charge curves (*OCV* and under load C/10 and 5 C) for Li|Li$^+$|Li$_x$Mn$_2$O$_4$ with cathode materials from solid-state reaction and sol–gel method. Charge curves for both materials have similar shape; however, they are differed by the polarization. The material from solid-state reaction exhibits much lower overpotential in the cell, especially visible when charged with higher currents. It can explained by better diffusion kinetics of material from SSR (Fig. 6a): higher capacities recorded for the cells assembled with this material as the better-conducting samples exhibit lower overpotentials in working cell. The results of electrochemical tests are in good agreement with lithium diffusion coefficients and confirm the influence of anomalous thermoelectric effects on the performance of a cathode.

Conclusions

It was shown that the synthesis method of LiMn$_2$O$_4$ has a crucial meaning for its properties, what affects the effectiveness of deintercalation/intercalation of lithium. The analysis of transport properties (conductivity, thermoelectric power, and chemical diffusion coefficient of lithium) in Li$_x$Mn$_2$O$_4$ cathode materials obtained by solid-state reaction and sol–gel method allows to formulate a conclusion that the performance of manganese spinel-based cathode depends on occurrence of anomalous electron effects. These distinctive peaks in thermoelectric power appear in the temperature of phase transition, where cubic to orthorhombic phase ratio is 1:1. The analysis of electronic structure calculation [23, 24] indicated on significant differences in density of states in both coexisting phases as a reason of occurrence of anomalous thermoelectric effects, what is more the recorded maxima in absolute values of thermoelectric power correspond to high diffusivity of electrons at

the Fermi level. Furthermore, a correlation between the occurrence of thermoelectric peaks and effectiveness of deintercalation/intercalation of lithium has been shown by comparing the values of these peaks with lithium diffusion coefficient, what would suggest that the origin of the differences of kinetic properties on both materials is of electronic origin and induced by the phase transition. Phase transition near the room temperature (i.e., Li-ion cell's working temperature) seems to be improving $Li_xMn_2O_4$-based cell performance.

Acknowledgements The work was realized by using the infrastructure of the Laboratory of Conversion and Energy Storage Materials in the Centre of Energy AGH.

Funding information The project was funded by the National Science Centre Poland (NCN) on the basis of the decision number UMO-2016/23/B/ST8/00199.

References

1. Goodenough JB, Manthiram A, Wnetrzewski B (1993) Electrodes for lithium batteries. J Power Sources 43(1-3):269–275
2. Sugiyama J, Tamura T, Yamauchi H (1995) Elastic/anelastic behaviour during the phase transition in spinel $LiMn_2O_4$. J Phys Condens Matter 7(50):9755–9764
3. Kondracki Ł, Kulka A, Milewska A, Molenda J (2017) In-situ structural studies of manganese spinel-based cathode materials. Electrochim Acta 227:294–302
4. Hayakawa H, Takada T, Enoki H, Akiba E (1998) New findings on the structural phase transitions of spinel $LiMn_2O_4$ at low temperature. J Mater Sci Lett 17(10):811–812
5. Rodriguez-Carvajal J, Rousse G, Masquelier C, Hervieu M (1998) Electronic crystallization in a lithium battery material: columnar ordering of electrons and holes in the spinel $LiMn_2O_4$. Phys Rev Lett 81(21):4660–4663
6. Huang H, Vincent CA, Bruce PG (1999) Correlating capacity loss of stoichiometric and nonstoichiometric lithium manganese oxide spinel electrodes with their structural integrity. J Electrochem Soc 146(10):3649–3654
7. Yamada A, Tanaka M, Tanaka K, Sekai K (1999) Jahn–Teller instability in spinel Li–Mn–O. J Power Sources 81:73–78
8. Wang GX, Bradhurst DH, Liu HK, Dou SX (1999) Improvement of electrochemical properties of the spinel $LiMn_2O_4$ using a Cr dopant effect. Solid State Ionics 120(1-4):95–101
9. Robertson AD, Lu SH, Averill WF, Howard WF (1997) M^{3+}-modified $LiMn_2O_4$ spinel intercalation cathodes I. Admetal effects on morphology and electrochemical performance. J Electrochem Soc 144(10):3500–3505
10. Kumagai N, Ooto H, Kumagai N (1997) Preparation and electrochemical characteristics of quaternary Li-Mn-VO spinel as the positive materials for rechargeable lithium batteries. J Power Sources 68(2):600–603
11. Striebel KA, Rougier A, Horne CR et al (1999) Electrochemical studies of substituted spinel thin films. J Electrochem Soc 146(12):4339–4347
12. Taniguchi I, Lim CK, Song D, Wakihara M (2002) Particle morphology and electrochemical performances of spinel $LiMn_2O_4$ powders synthesized using ultrasonic spray pyrolysis method. Solid State Ionics 146(3-4):239–247
13. Shigemura H, Sakaebe H, Kageyama H, Kobayashi H, West AR, Kanno R, Morimoto S, Nasu S, Tabuchi M (2001) Structure and electrochemical properties of $LiFe_xMn_{2-x}O_4$ ($0 \leqslant x \leqslant 0.5$) spinel as 5 V electrode material for lithium batteries. J Electrochem Soc 148(7):A730–A736
14. Hwang K-T, Um W-S, Lee H-S, Song JK, Chung KW (1998) Powder synthesis and electrochemical properties of $LiMn_2O_4$ prepared by an emulsion-drying method. J Power Sources 74(2):169–174
15. Wang L, Li H, Huang X (2012) Electrochemical properties and interfacial reactions of LiNi0.5Mn1.5O4−δ nanorods. Prog Nat Sci Mater Int 22(3):207–212
16. Larcher D, Gérand B, Tarascon J-M (1998) Synthesis and electrochemical performances of Li 1+ y Mn 2− y O 4 powders of well-defined morphology. J Solid State Electrochem 2(3):137–145
17. Amatucci GG, Pereira N, Zheng T et al (1999) Enhancement of the electrochemical properties of $Li_1Mn_2O_4$ through chemical substitution. J Power Sources 81:39–43
18. Molenda J, Marzec J, Świerczek K et al (2004) The effect of 3d substitutions in the manganese sublattice on the charge transport mechanism and electrochemical properties of manganese spinel. Solid State Ionics 171(3-4):215–227
19. Molenda J, Pałubiak D, Marzec J (2005) Transport and electrochemical properties of the Li y Cr x Mn 2− x O 4 (0< x< 0.5) cathode material. J Power Sources 144(1):176–182
20. Molenda J, Świerczek K, Marzec J, Liu RS (2003) Charge transport mechanism in $LiCo_yMn_{2-y}O_4$ cathode material. Solid State Ionics 157(1-4):101–108
21. Molenda J, Ojczyk W, Marzec M et al (2003) Electrochemical and chemical deintercalation of $LiMn_2O_4$. Solid State Ionics 157(1-4):73–79
22. Molenda J, Świerczek K, Molenda M, Marzec J (2000) Electronic structure and reactivity of $Li_{1-x}Mn_2O_4$ cathode. Solid State Ionics 135(1-4):53–59
23. Grechnev GE, Ahuja R, Johansson B, Eriksson O (2002) Electronic structure, magnetic, and cohesive properties of $Li_xMn_2O_4$: theory. Phys Rev B 65(17):174408
24. Grechnev GE, Ahuja R, Johansson B, Eriksson O (2003) Electronic structure and magnetic properties of lithium manganese spinels. J Magn Magn Mater 258:287–289
25. Molenda J, Marzec J, Świerczek K et al (2004) The effect of 3d substitutions in the manganese sublattice on the electrical and electrochemical properties of manganese spinel. Solid State Ionics 175(1-4):297–304
26. Milewska A, Kondracki L, Molenda M, Bakierska M, Molenda J (2014) Structural, transport and electrochemical properties of

$LiNi_{0.5-y}Cu_yMn_{1.5}O_{4-delta}$ spinel cathode materials. Solid State Ionics 267:27–31
27. Larson AC, Von Dreele RB (2000) General structure analysis system (GSAS). Los Alamos Natl Lab Rep LAUR:86–748
28. Weppner W, Huggins RA (1977) Determination of kinetic and thermodynamic parameters of mixed-conducting electrodes, and application to system Li-Sb. J Electrochem Soc 124(10):1569–1578
29. Deiss E (2005) Spurious chemical diffusion coefficients of Li^+ in electrode materials evaluated with GITT. Electrochim Acta 50(14): 2927–2932
30. Shaju KM, Subba Rao GV, Chowdari BVR (2003) Li ion kinetic studies on spinel cathodes, $Li(M_{1/6}Mn_{11/6})O_4$ (M = Mn, Co, CoAl) by GITT and EIS. J Mater Chem 13(1):106–113
31. Kim S, Pyun S (2002) Analysis of cell impedance measured on the $LiMn_2O_4$ film electrode by PITT and EIS with Monte Carlo simulation. J Electroanal Chem 528(1-2):114–120
32. Xie J, Kohno K, Matsumura T, Imanishi N, Hirano A, Takeda Y, Yamamoto O (2008) Li-ion diffusion kinetics in $LiMn_2O_4$ thin films prepared by pulsed laser deposition. Electrochim Acta 54(2):376–381
33. Tang SB, Lai MO, Lu L (2008) Study on Li^+-ion diffusion in nanocrystalline $LiMn_2O_4$ thin film cathode grown by pulsed laser deposition using CV, EIS and PITT techniques. Mater Chem Phys 111(1):149–153